Error Estimation of the Cauer Ladder Network Method for the Time-domain Analysis and Its Application to a Multiport System

Miwa Tobita[1], Stéphane Clénet[2], Shingo Hiruma[1], Wei Chen[2], and Tetsuji Matsuo[1]
[1] Graduate School of Engineering, Kyoto University, Kyoto 6158510, Japan
[2] L2EP, Centrale Lille, Arts et Métiers Sciences and Technologies, HEI, Université de Lille, Lille 59000, France

The Cauer ladder network (CLN) method can accelerate eddy current field analysis of electromagnetic devices in the time domain by reducing the order of the finite element (FE) model. To control its accuracy, the reduction error should be estimated without conducting the FE analysis. In this study, we extend the estimation method in the frequency domain developed in a previous study to time-domain analysis. The proposed method is also extended to a multiport system. Numerical examples illustrate that the proposed error estimation method is effective.

***Index Terms*—Cauer ladder network (CLN), error estimation, time-domain analysis, eddy current field analysis, model order reduction (MOR).**

I. Introduction

Model order reduction (MOR) methods have been employed to speed up eddy current field analysis of electromagnetic devices [1]. The Cauer ladder network (CLN) method [2]–[6] is a prominent candidate for MOR in quasistatic field analysis. It reduces the electromagnetic field distribution to basis vectors, which determine the circuit elements of the ladder network. A CLN can be easily coupled with other systems modeled by electrical circuits, such as control systems. Theoretically, an infinitely continued ladder network provides a solution identical to that of the full model, whereas a network truncated at the N-th stage provides a reduced model whose number of unknowns is N.

The estimation of errors arising from model reduction has been studied extensively [7], [8]. Regarding the CLN method, previous studies [5], [6] have developed error estimation methods to evaluate the reduction error and determine the number of stages of CLN by exploiting the formulation of the CLN method. However, they are only valid in the frequency domain. Application to the time domain is frequently required in numerous cases, such as in the evaluation of control strategies. In this context, this study aims to extend the formulation of the error estimation presented in [5] to the time domain.

Moreover, although [5] considered only a single-port system, electromagnetic devices often have multiple input and output ports. Magnetic coupling among the ports should also be considered; hence, we extend the proposed method to the case of a multiport CLN [3].

II. The Error Estimation Method in Time Domain

A. Formulation

The discretized form of the governing equations of the eddy current field in finite element (FE) space is given as follows:

$$\boldsymbol{C}\boldsymbol{e}_{\mathrm{FE}} = -\boldsymbol{\mu}\frac{\mathrm{d}\boldsymbol{h}_{\mathrm{FE}}}{\mathrm{d}t}, \quad \boldsymbol{C}^{\mathrm{T}}\boldsymbol{h}_{\mathrm{FE}} = \boldsymbol{\sigma}\boldsymbol{e}_{\mathrm{FE}}. \tag{1}$$

Corresponding author: M. Tobita (email: tobita.miwa.73x@kyoto-u.jp).

where $\boldsymbol{C}$ is the edge-face incidence matrix; $\boldsymbol{e}_{\mathrm{FE}}$ and $\boldsymbol{h}_{\mathrm{FE}}$ are the FE discretization of the electric and magnetic fields, respectively; and $\boldsymbol{\mu}$ and $\boldsymbol{\sigma}$ are matrix representations of the permeability and conductivity, respectively, discretized in the FE space. They are constants assuming linear material properties.

A single-port CLN truncated at the $(N+1)$-th stage is shown in Fig. 1(a), where R_{2n} and L_{2n+1} $(n = 0, \cdots, N)$ are the resistance and inductance elements, respectively. State vectors V_{2n} and I_{2n+1} are the voltage across R_{2n} and current flowing through L_{2n+1}, respectively. The approximate solution of the electric and magnetic fields $\boldsymbol{e}^N$ and $\boldsymbol{h}^N$ can be obtained by

$$\boldsymbol{e}^N = \sum_{n=0}^{N} V_{2n}\boldsymbol{e}_{2n}, \quad \boldsymbol{h}^N = \sum_{n=0}^{N} I_{2n+1}\boldsymbol{h}_{2n+1}, \tag{2}$$

where $\boldsymbol{e}_{2n}$ and $\boldsymbol{h}_{2n+1}$ are the basis vectors of the electric and magnetic fields, respectively, which are determined by applying the CLN recurrence procedure [2]. We also introduce

$$\boldsymbol{e}_+^N = \boldsymbol{e}^N + V_{2N+2}\boldsymbol{e}_{2N+2} = \sum_{n=0}^{N+1} V_{2n}\boldsymbol{e}_{2n} \tag{3}$$

for the error estimation, where $V_{2N+2} = L_{2N+1}\mathrm{d}I_{2N+1}/\mathrm{d}t$ is defined as the voltage across the resistance R_{2N+2} added to the $(N+2)$-th stage for the error estimation (Fig. 1(b)).

Vector pairs $(\boldsymbol{h}^N, \boldsymbol{e}_+^N)$ and $(\boldsymbol{h}^N, \boldsymbol{e}^N)$ satisfy

$$\boldsymbol{C}\boldsymbol{e}_+^N = -\boldsymbol{\mu}\frac{\mathrm{d}\boldsymbol{h}^N}{\mathrm{d}t}, \quad \boldsymbol{C}^{\mathrm{T}}\boldsymbol{h}^N = \boldsymbol{\sigma}\boldsymbol{e}^N, \tag{4}$$

whose derivation is provided in Appendix A. This derivation extends the work of [5] from the frequency domain to the time domain.

The objective of the error estimation method proposed here is to determine the upper bound of the reduction error of the $(N+1)$-stage CLN

$$\epsilon_{\mathrm{MOR}}^2 = \|\boldsymbol{e}^N - \boldsymbol{e}_{\mathrm{FE}}\|_\sigma^2 \tag{5}$$

without conducting a transient FE analysis to obtain $\boldsymbol{e}_{\mathrm{FE}}$. Here, $\|\boldsymbol{X}\|_\sigma^2 = \boldsymbol{X}^{\mathrm{T}}\boldsymbol{\sigma}\boldsymbol{X}$ represents the energy norm of vector

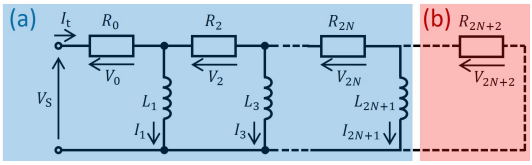

Fig. 1. (a) $(N+1)$-stage CLN and (b) additional resistance used for the definition of the error estimator.

$\boldsymbol{X}$. To achieve the aforementioned target, we define the error estimator of the electric field as

$$\epsilon_{\rm est}^2 = \|\boldsymbol{e}_+^N - \boldsymbol{e}^N\|_\sigma^2 = \|V_{2N+2}\boldsymbol{e}_{2N+2}\|_\sigma^2 = \frac{V_{2N+2}^2}{R_{2N+2}}. \tag{6}$$

It can be computed inexpensively because only an integral operation in the FE space and some algebraic operations are required to obtain R_{2N+2} and V_{2N+2}, respectively, in addition to the normal CLN calculation. The estimator can be expanded using $\boldsymbol{e}_{\rm FE}$:

$$\begin{aligned}\epsilon_{\rm est}^2 &= \|(\boldsymbol{e}_+^N - \boldsymbol{e}_{\rm FE}) + (\boldsymbol{e}_{\rm FE} - \boldsymbol{e}^N)\|_\sigma^2 \\ &= \|\boldsymbol{e}_+^N - \boldsymbol{e}_{\rm FE}\|_\sigma^2 + \epsilon_{\rm MOR}^2 + 2(\boldsymbol{e}_+^N - \boldsymbol{e}_{\rm FE})^{\rm T}\boldsymbol{\sigma}(\boldsymbol{e}_{\rm FE} - \boldsymbol{e}^N) \\ &= M + C, \end{aligned} \tag{7}$$

where the main terms $M = \|\boldsymbol{e}_+^N - \boldsymbol{e}_{\rm FE}\|_\sigma^2 + \epsilon_{\rm MOR}^2$ also appear in the frequency domain [5], and $C = 2(\boldsymbol{e}_+^N - \boldsymbol{e}_{\rm FE})^{\rm T}\boldsymbol{\sigma}(\boldsymbol{e}_{\rm FE} - \boldsymbol{e}^N)$ is newly defined here as a cross term. Substituting (1) and (4) into C, we obtain

$$\begin{aligned} C &= 2\left[\frac{\rm d}{{\rm d}t}(\boldsymbol{h}_{\rm FE} - \boldsymbol{h}^N)\right]^{\rm T}\boldsymbol{\mu}(\boldsymbol{h}_{\rm FE} - \boldsymbol{h}^N) \\ &= \frac{\rm d}{{\rm d}t}\|\boldsymbol{h}^N - \boldsymbol{h}_{\rm FE}\|_\mu^2, \end{aligned} \tag{8}$$

where $\|\boldsymbol{X}\|_\mu^2 = \boldsymbol{X}^{\rm T}\boldsymbol{\mu}\boldsymbol{X}$. The average of C over one electrical period becomes zero for periodic solutions, which implies that the cross term vanishes in the frequency-domain analysis.

Let us assume the initial condition $\boldsymbol{h}^N = \boldsymbol{h}_{\rm FE} = \boldsymbol{0}$, and define the average of M and C over the time interval $[0, t]$ as

$$F_{\rm M}(t) = \frac{1}{t}\int_0^t M{\rm d}\tau, \tag{9}$$

$$F_{\rm C}(t) = \frac{1}{t}\int_0^t C{\rm d}\tau = \frac{1}{t}\|\boldsymbol{h}^N - \boldsymbol{h}_{\rm FE}\|_\mu^2|_t \geq 0, \tag{10}$$

respectively, where $t > 0$. We also introduce the notation for time-averaged errors, as follows:

$$F_{\rm MOR}(t) = \frac{1}{t}\int_0^t \epsilon_{\rm MOR}^2{\rm d}\tau, \quad F_{\rm est}(t) = \frac{1}{t}\int_0^t \epsilon_{\rm est}^2{\rm d}\tau. \tag{11}$$

From (7)–(11), we obtain the upper bound of the reduction error $F_{\rm MOR}$ as

$$F_{\rm est}(t) = F_{\rm M}(t) + F_{\rm C}(t) \geq F_{\rm MOR}(t). \tag{12}$$

The overall influence of the residue is negligible when the ratio $G(t)$ of the cross term to main terms is small, i.e.,

$$G(t) = F_{\rm C}(t)/F_{\rm M}(t) \ll 1 \tag{13}$$

is satisfied.

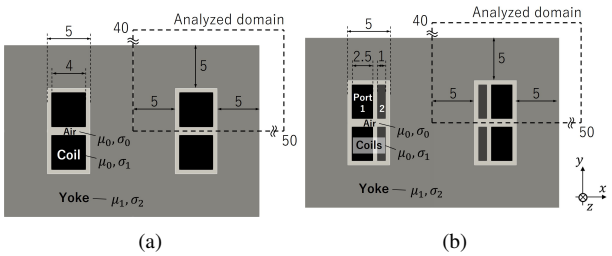

Fig. 2. Two-dimentional bulk-core inductor model used in the numerical analyses of (a) single-port and (b) multiport system. The unit of dimensions is mm.

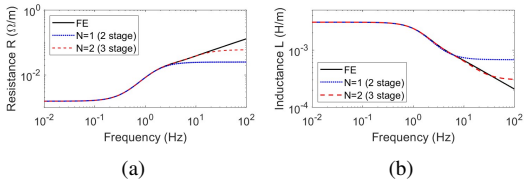

Fig. 3. (a) Resistance and (b) inductance of the single-port inductor model computed using the FE and CLN methods. Lines $N = 1$ and 2 were obtained using two- and three-stage CLN terminated at L_3 and L_5, respectively.

B. Numerical Example

Numerical analyses were conducted using a bulk iron-core inductor, as shown in Fig. 2(a). The permeability and conductivity were $(\mu_0, \mu_1) = (4\pi \times 10^{-7}, 4\pi \times 10^{-3})$ H/m and $(\sigma_0, \sigma_1, \sigma_2) = (0, 4.0 \times 10^7, 1.0 \times 10^6)$ S/m, respectively. Fig. 3 shows the frequency dependence of resistance $R = {\rm Re}(Z)$ and inductance $L = {\rm Im}(Z)/2\pi f$, where Z is the impedance of the model. The resistance starts to increase at approximately 0.2 Hz, above which the skin effect is observable. Additionally, the inductance starts to decrease at around 1 Hz; at higher frequencies, the model fails to operate as an inductor in practice.

The implicit Euler scheme was adopted to solve the time evolution in both CLN and FE analyses with the same time step. We chose a sufficiently small time step to neglect the error originating from the discretization in time. A two-stage CLN ($N = 1$) was constructed from the FE model using the CLN recurrence procedure.

1) Sinusoidal Input

A sinusoidal electric field input $0.3\sin(2\pi ft)$ V/m was applied to the coil in z-direction, where f is the frequency. The simulation was conducted from $t = 0$ to $3T$, where $T = 1/f$ is the electrical period.

Fig. 4(a) shows the time evolution of the reduction error of the two-stage CLN $\epsilon_{\rm MOR}^2$, error estimator $\epsilon_{\rm est}^2$, and absolute value of the cross term $|C|$ (see (5)–(8)) normalized by $\|\boldsymbol{e}_{\rm FE}\|_\sigma^2$ at each time step when $f = 10$ Hz. The absolute value of C was much lower than $\epsilon_{\rm est}^2$, which suggests that the influence of the cross term was not significant. The estimator $\epsilon_{\rm est}^2$ was larger than the reduction error $\epsilon_{\rm MOR}^2$ most of the time. Although $\epsilon_{\rm MOR}^2$ was larger than $\epsilon_{\rm est}^2$ for short durations (see the enlarged figure in Fig. 4) due to the influence of the cross term, this occurred only when the error itself was small enough to be insignificant. Fig. 4(b) shows the ratio of the cross term

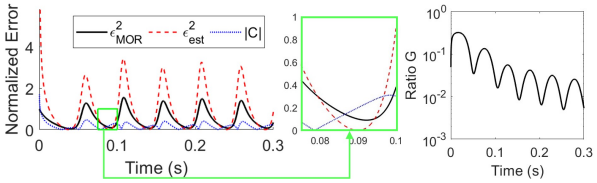

(a) (b)

Fig. 4. (a) Time evolution of the reduction error $\epsilon^2_{\mathrm{MOR}}$, error estimator $\epsilon^2_{\mathrm{est}}$, and absolute value of the cross term $|C|$ normalized by $\|\boldsymbol{e}_{\mathrm{FE}}\|^2_\sigma$. The input frequency is 10 Hz. (b) Time evolution of the ratio G at 10 Hz. It decreases with time because the influence of the cross term becomes smaller.

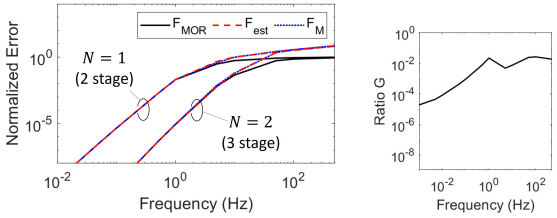

(a) (b)

Fig. 5. (a) The time-averaged reduction error F_{MOR}, error estimator F_{est}, and its main part F_{M} ($N = 1, 2$) at $t = 3T$ across different frequencies. (b) The ratio G at $t = 3T$.

to the main term $G(t)$ changing with time at 10 Hz. When $t < T = 0.1$ s, the cross term had a visible influence, with G as high as 0.3, whereas it diminished for a larger t.

Fig. 5(a) shows F_{e}, F_{M}, F_{est}, and F_{MOR} (see (9)–(11)) at $t = 3T$ for various frequencies. The relationship $F_{\mathrm{est}} \approx F_{\mathrm{M}} \geq F_{\mathrm{MOR}}$ was observed, indicating that (12) and (13) were satisfied. The upper bound of the time-averaged error F_{MOR} was properly obtained using F_{est}. Fig. 5(a) also shows errors with a larger number of stages ($N = 2$, three-stage CLN). As expected, the error decreased as the number of stages, that is, the order of the reduced system, increased. The error estimator allows us to determine the necessary number of stages by considering an acceptable level of error in the analysis.

Fig. 5(b) shows ratio G in (13) at $t = 3T$. The highest value was 0.03, which was sufficiently low to ensure that the effect of the cross term was negligible.

2) PWM Input

We also applied pulse width modulation (PWM) input, where a sine waveform (1 Hz) was compared with a carrier triangular waveform. Fig. 6 shows the normalized $\epsilon^2_{\mathrm{MOR}}$, $\epsilon^2_{\mathrm{est}}$, and $|C|$ when the carrier frequency is 45 Hz. At the moment of switching, the cross term $|C|$, which is the time differentiation of $\|\boldsymbol{h}^N - \boldsymbol{h}_{\mathrm{FE}}\|^2_\mu$ (refer to (8)), exhibited a significant increase. The estimator $\epsilon^2_{\mathrm{est}}$ consistently offered an upper bound for $\epsilon^2_{\mathrm{MOR}}$ in every instance in this case.

Fig. 7(a) shows the time-averaged errors F_{MOR}, F_{est}, and F_{M} at $t = 3T$ with carrier frequencies of 9, 45, and 225 Hz. The condition $F_{\mathrm{est}} \approx F_{\mathrm{M}} \geq F_{\mathrm{MOR}}$ was satisfied, which validated the effectiveness of the proposed method even for PWM inputs.

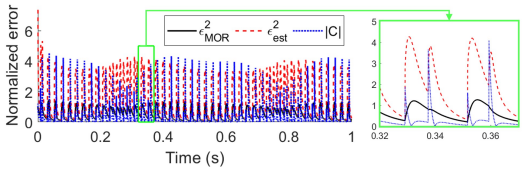

Fig. 6. Time evolution of $\epsilon^2_{\mathrm{MOR}}$, $\epsilon^2_{\mathrm{est}}$, and $|C|$ with the PWM input of its carrier frequency 45 Hz.

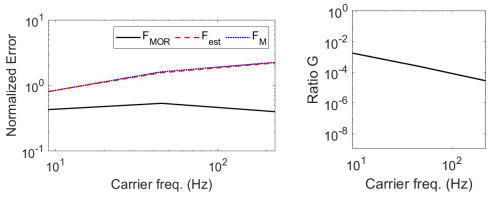

(a) (b)

Fig. 7. (a) Time-averaged errors F_{MOR}, F_{est}, and F_{M} with $t = 3T$ when the PWM inputs are supplied. (b) The ratio G at $t = 3T$.

III. Extension to Multiport CLN

A. Formulation

Realistic applications include simulations of multi-input, multi-output devices such as motors and transformers. The error estimation method presented thus far for a single input can also be applied to a multiport CLN [3] with almost the same formulation. Let P be the number of ports in a ladder network, whose circuit matrices are $\boldsymbol{R}_{2n}, \boldsymbol{L}_{2n+1} \in \mathbb{R}^{P\times P}$ and voltage and current vectors are $\boldsymbol{V}_{2n}, \boldsymbol{I}_{2n+1} \in \mathbb{R}^P$. Using the same approach as the single-port system, the electric and magnetic fields are reconstructed from an $(N+1)$-stage multiport CLN (Fig. 8(a)) as $\boldsymbol{e}^N = \sum_{n=0}^N \boldsymbol{e}_{2n}\boldsymbol{V}_{2n}$ and $\boldsymbol{h}^N = \sum_{n=0}^N \boldsymbol{h}_{2n+1}\boldsymbol{I}_{2n+1}$, respectively, where $\boldsymbol{e}_{2n} = [\boldsymbol{e}_{1,2n}, \boldsymbol{e}_{2,2n}, \cdots, \boldsymbol{e}_{P,2n}]$ and $\boldsymbol{h}_{2n+1} = [\boldsymbol{h}_{1,2n+1}, \boldsymbol{h}_{2,2n+1}, \cdots, \boldsymbol{h}_{P,2n+1}]$. Here, $\boldsymbol{e}_{p,2n}$ and $\boldsymbol{h}_{p,2n+1}$ ($p = 1, 2, \cdots, P$) are the $2n$-th and $(2n+1)$-th basis vectors of the electric and magnetic fields, respectively, when the unit input is provided only to the p-th port. We also define $\boldsymbol{e}^N_+$ as $\boldsymbol{e}^N_+ = \sum_{n=0}^{N+1} \boldsymbol{e}_{2n}\boldsymbol{V}_{2n}$, where $\boldsymbol{V}_{2N+2} = \boldsymbol{L}_{2N+1}\mathrm{d}\boldsymbol{I}_{2N+2}/\mathrm{d}t$ denotes the voltage across the additional resistance matrix $\boldsymbol{R}_{2N+2}$ as shown in Fig. 8(b). As was the case with the single-port CLN, ($\boldsymbol{h}^N$, $\boldsymbol{e}^N_+$) and ($\boldsymbol{h}^N$, $\boldsymbol{e}^N$) satisfy (4), as shown in Appendix A, when linear material characteristics are assumed.

The error estimator of the electric field is given by

$$\begin{aligned}\epsilon^2_{\mathrm{est}} &= \|\boldsymbol{e}^N_+ - \boldsymbol{e}^N\|^2_\sigma = \|\boldsymbol{e}_{2N+2}\boldsymbol{V}_{2N+2}\|^2_\sigma \\ &= \boldsymbol{V}^{\mathrm{T}}_{2N+2}\boldsymbol{R}^{-1}_{2N+2}\boldsymbol{V}_{2N+2},\end{aligned} \tag{14}$$

where the energy norm $\|\boldsymbol{X}\|^2_\sigma$ is calculated in the same manner as in single-port CLN. Moreover, formulations identical to those of the single-port CLN are obtained for $\epsilon^2_{\mathrm{MOR}}$, M and C and the time-averaged errors F_{MOR}, F_{est}, F_{M}, and F_{C}.

B. Numerical Example

We employed the multiport inductor model shown in Fig. 2(b) in Section II. The coils were divided into two regions, each of which represents a port component. The applied

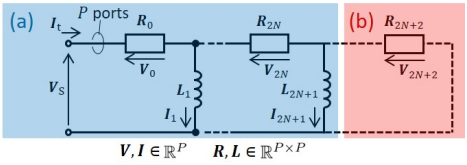

Fig. 8. (a) $(N+1)$-stage multiport CLN and (b) additional resistance matrix used in the error estimation.

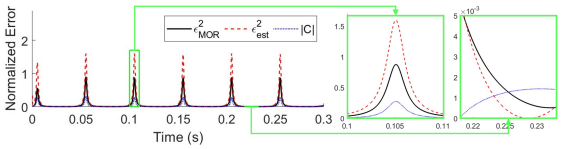

Fig. 9. Time evolution of $\epsilon^2_{\mathrm{MOR}}$, $\epsilon^2_{\mathrm{est}}$, and $|C|$ of the multiport CLN, where the input frequency is 10 Hz.

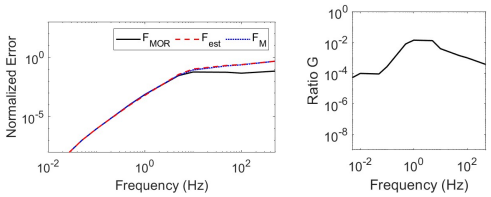

(a) (b)

Fig. 10. (a) Time-averaged errors F_{MOR}, F_{est}, and F_{M} of the multiport CLN at various frequencies with $t = 3T$. (b) The ratio G at $t = 3T$.

inputs were z-directional electric fields $0.3\cos(2\pi ft)$ and $0.1\sin(2\pi ft)$ V/m for the first and second ports, respectively.

Fig. 9 shows the time evolutions of $\epsilon^2_{\mathrm{MOR}}$, $\epsilon^2_{\mathrm{est}}$, and $|C|$ for an input frequency of 10 Hz. As was the case with the single-port CLN, the estimator $\epsilon^2_{\mathrm{est}}$ was larger than $\epsilon^2_{\mathrm{MOR}}$ in most instances (see the first enlarged figure), except when the error was extremely low (the second enlarged figure).

Fig. 10(a) shows F_{MOR}, F_{est}, and F_{M} at $t = 3T$ at various frequencies. The relationship $F_{\mathrm{est}} \approx F_{\mathrm{M}} \geq F_{\mathrm{MOR}}$ was satisfied. Fig. 10(b) shows ratio G at $t = 3T$. The highest value was 0.01, indicating that the cross term was negligible.

IV. Conclusions

This study extended the existing error estimation formulation for the CLN method to time-domain analysis, including the analysis of multiport devices. We showed that the error estimator contains a cross term that vanishes in frequency-domain analysis. Moreover, the numerical examples indicated that the influence of the cross term on time-averaged errors was negligible. For both single-port and multiport CLNs, the upper bound of the time-averaged reduction error was successfully obtained by the estimator as intended.

Appendix A

Equation (4) is derived below under the assumption of an P-port system, which becomes a single-port system when $P = 1$. The CLN recurrence formula yields

$$\boldsymbol{C}\boldsymbol{e}_{2n} = -\sum_{k=0}^{n-1} \boldsymbol{\mu}\boldsymbol{h}_{2k+1}\boldsymbol{L}^{-1}_{2k-1},\ \boldsymbol{C}^{\mathrm{T}}\boldsymbol{h}_{2n+1} = \sum_{k=0}^{n} \boldsymbol{\sigma}\boldsymbol{e}_{2k}\boldsymbol{R}_{2k}. \quad (15)$$

When the magnetic characteristics are linear, the circuit equations of the CLN are represented as

$$\sum_{k=n}^{N+1} \boldsymbol{V}_{2k} = \boldsymbol{L}_{2n-1}\frac{\mathrm{d}\boldsymbol{I}_{2n-1}}{\mathrm{d}t},\quad \sum_{k=n}^{N} \boldsymbol{I}_{2k+1} = \boldsymbol{R}^{-1}_{2n}\boldsymbol{V}_{2n}. \quad (16)$$

Using (15) and (16), we can expand $\boldsymbol{C}\boldsymbol{e}^N_+$ as

$$\begin{aligned}
\boldsymbol{C}\boldsymbol{e}^N_+ &= \sum_{n=0}^{N+1} \boldsymbol{C}\boldsymbol{e}_{2n}\boldsymbol{V}_{2n} \\
&= \sum_{n=0}^{N+1}\left(\sum_{k=0}^{n-1} -\boldsymbol{\mu}\boldsymbol{h}_{2k+1}\boldsymbol{L}^{-1}_{2k+1}\right)\boldsymbol{V}_{2n} \\
&= -\sum_{k=0}^{N} \boldsymbol{\mu}\boldsymbol{h}_{2k+1}\boldsymbol{L}^{-1}_{2k+1}\left(\sum_{n=k+1}^{N+1}\boldsymbol{V}_{2n}\right) \\
&= -\boldsymbol{\mu}\sum_{k=0}^{N}\frac{\mathrm{d}}{\mathrm{d}t}\left(\boldsymbol{h}_{2k+1}\boldsymbol{I}_{2k+1}\right) = -\boldsymbol{\mu}\frac{\mathrm{d}\boldsymbol{h}^N}{\mathrm{d}t}, \qquad (17)
\end{aligned}$$

which is the second equation in (4). Similarly, the first equation can be derived as

$$\begin{aligned}
\boldsymbol{C}^{\mathrm{T}}\boldsymbol{h}^N &= \sum_{n=0}^{N} \boldsymbol{C}^{\mathrm{T}}\boldsymbol{h}_{2n+1}\boldsymbol{I}_{2n+1} \\
&= \sum_{n=0}^{N}\left(\sum_{k=0}^{n} \boldsymbol{\sigma}\boldsymbol{e}_{2k}\boldsymbol{R}_{2k}\right)\boldsymbol{I}_{2n+1} \\
&= \sum_{k=0}^{n} \boldsymbol{\sigma}\boldsymbol{e}_{2k}\boldsymbol{R}_{2k}\left(\sum_{n=k}^{N}\boldsymbol{I}_{2n+1}\right) \\
&= \boldsymbol{\sigma}\sum_{k=0}^{n}\boldsymbol{e}_{2k}\boldsymbol{V}_{2k} = \boldsymbol{\sigma}\boldsymbol{e}^N. \qquad (18)
\end{aligned}$$

Acknowledgment

This work was supported by JSPS KAKENHI Grant Numbers 20K04443 and 23KJ1202 and JSPS Invitational Fellowships for Research in Japan (Long Term).

References

[1] MD. R. Hasan, L. Montier, T. Henneron, and R. V. Sabariego, "Stabilized Reduced-Order Model of a Non-Linear Eddy Current Problem by a Gappy-POD Approach," *IEEE Trans. Magn.,* vol. 54, no. 12, Art. no. 8001808, 2018.

[2] A. Kameari, H. Ebrahimi, K. Sugahara, Y. Shindo, and T. Matsuo, "Cauer ladder network representation of eddy-current fields for model order reduction using finite-element method," *IEEE Trans. Magn.,* vol. 54, no. 3, Art no. 7201804, 2018.

[3] T. Matsuo et al., "Multi-port model order reduction using a matrix cauer ladder network," *IEEE Trans. Magn.,* vol. 56, no. 2, Art. no. 7506905, 2020.

[4] N. Koester, O. Koenig, A. Thaler, and O. Bíró, "Application of model order reduction with Cauer ladder networks to industrial inductors," *COMPEL,* vol. 41, no. 3, pp. 867–877, 2021.

[5] S. Hiruma, S. Clénet, H. Igarashi, and T. Henneron, "Error Estimator for Cauer Ladder Network Representation," *IEEE Trans. Magn.,* vol. 58, no. 9, Art no. 7500904, 2022.

[6] H. Nagamine, S. Hiruma, T. Mifune, and T. Matsuo, "Error Estimation of the Cauer Ladder Network Method Based on Eigenfunction Expansion," *IEEE Trans. Magn.,* vol. 59, no. 5, Art no. 7001604, 2023.

[7] Z. Bai, R. D. Slone, W. T. Smith, and Q. Ye, "Error bound for reduced system model by Padápproximation via the Lanczos process," *IEEE TCAD,* vol. 18, no. 2, pp. 133–141, 1999.

[8] S. Chaturantabut and D. C. Sorensen, "A State Space Error Estimate for POD-DEIM Nonlinear Model Reduction," *SIAM J. Numer. Anal.,* vol. 50, no. 1, pp. 46–63, 2012.